Volume 24
Number 29
7 August 2022
Pages 17365–17902

PCCP

Physical Chemistry Chemical Physics

rsc.li/pccp

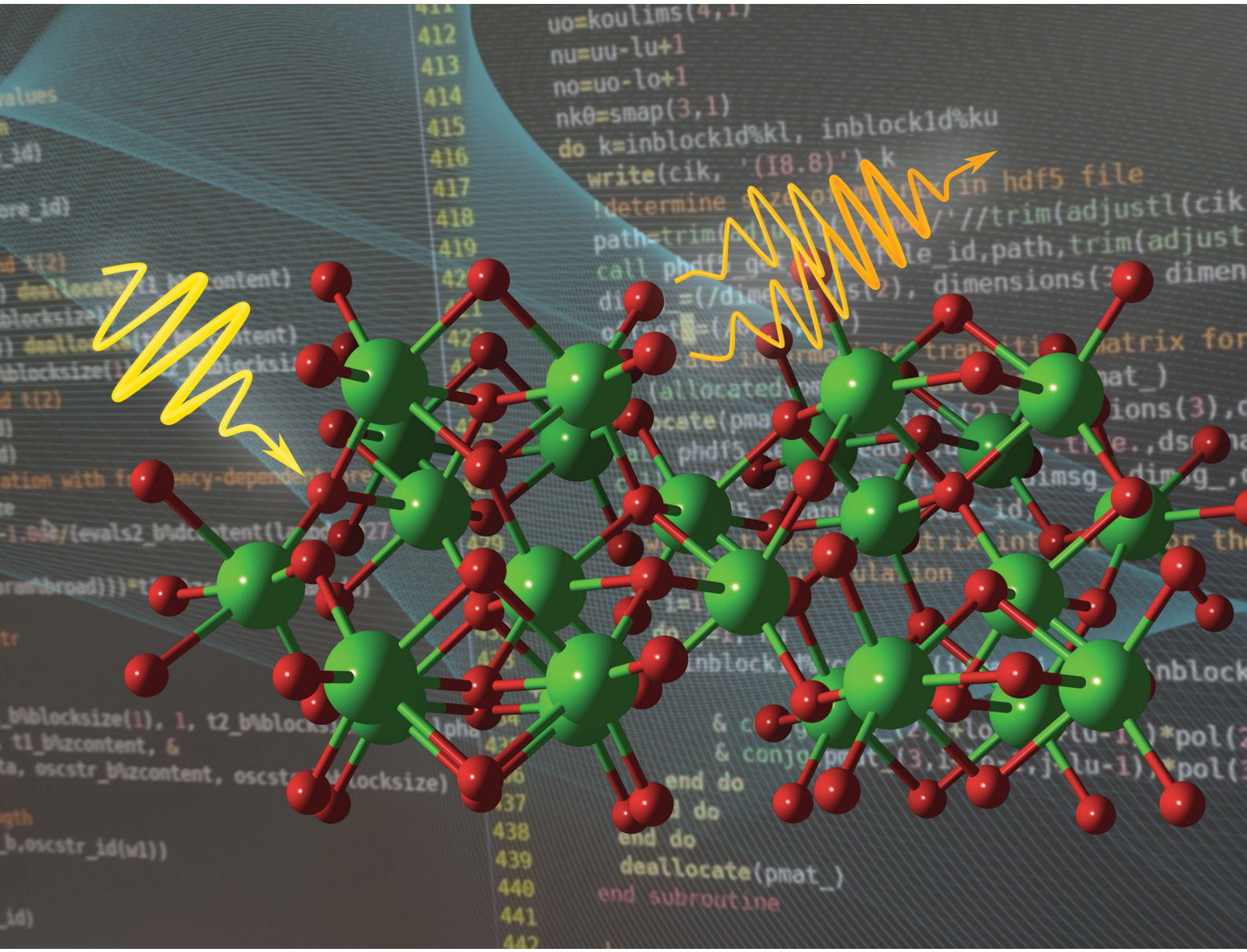

ISSN 1463-9076

ROYAL SOCIETY OF CHEMISTRY

PAPER

Claudia Draxl *et al.*

All-electron many-body approach to resonant inelastic X-ray scattering

PCCP

PAPER

View Article Online
View Journal | View Issue

Cite this: *Phys. Chem. Chem. Phys.*, 2022, **24**, 17439

Received 1st March 2022,
Accepted 11th May 2022

DOI: 10.1039/d2cp00994c

rsc.li/pccp

All-electron many-body approach to resonant inelastic X-ray scattering

Christian Vorwerk, †[a] Francesco Sottile [b] and Claudia Draxl*[a]

We present a formalism for the resonant inelastic X-ray scattering (RIXS) cross section. The resulting compact expression in terms of polarizability matrix elements, particularly lends itself to the implementation in an all-electron many-body perturbation theory (MBPT) framework, which is realized in the full-potential package `exciting`. With the carbon K edge RIXS of diamond and the oxygen K edge RIXS of β-Ga_2O_3, respectively, we demonstrate the importance of electron-hole correlation and atomic coherence in the RIXS spectra.

1 Introduction

Resonant inelastic X-ray scattering (RIXS) is a "photon-in-photon-out" scattering process, consisting of a coherent X-ray absorption and X-ray emission process.[1,2] The energy difference between the absorbed and emitted X-ray photons is transferred to the system. Being bulk-sensitive, element- and orbital-specific and giving access to a large scattering phase space, RIXS has become a widely used experimental probe of elementary excitations in molecules[3–5] and solids.[1,2,6,7] Accurate *ab initio* simulations can provide insight into the complex RIXS process and predict the corresponding spectra. In this context, the electron-hole correlations of the X-ray absorption and emission processes as well as the quantum coherence between them is a challenge for *ab initio* approaches.

For the first-principles calculations of both valence and core excitations in solids, the Bethe–Salpeter equation (BSE) formalism[8–13] has become the state of the art in recent decades. However, only few applications of the BSE formalism to RIXS[14–20] have been presented so far. All of them relied on the pseudopotential approximation where only selected valence and conduction orbitals are explicitly included in the calculation, while more strongly-bound electrons are only treated implicitly through the pseudopotential. The wavefunctions required for the calculations of X-ray absorption and scattering in these BSE implementations[14,18,21–23] rely on the pseudopotential approximations *via* the projector augmented-wave method.[24–27]

In this work, we go beyond by presenting an all-electron full-potential BSE approach to RIXS. We derive a compact analytical expression of the RIXS cross section within many-body perturbation theory (MBPT) that contains both the effects of electron-hole correlation and of the quantum coherence of the resonant scattering. We have implemented this novel expression in the all-electron many-body perturbation theory code `exciting`,[28–30] where we make use of consistent BSE calculations of core and valence excitations, based on the explicit access to core, valence, and conduction orbitals and matrix elements between them. To demonstrate our approach, we have chosen two representative examples: In the carbon K edge of diamond, we particularly study the influence of electron-hole correlation, while in the oxygen K edge of β-Ga_2O_3, we show how the coherence between excitations at different atomic sites impacts the RIXS spectra.

2 Theory

The double-differential cross section (DDCS) $d^2\sigma/d\Omega_2 d\omega_2$ for the scattering of a photon with energy ω_1, polarization e_1, and momentum K_1 into a photon with energy ω_2, polarization e_2, and momentum K_2 is given by the generalized Kramers–Heisenberg[31] formula

$$\frac{d^2\sigma}{d\Omega_2 d\omega_2} = \alpha^4 \left(\frac{\omega_2}{\omega_1}\right) \sum_f \left| \langle f|\mathbf{e}_1 \cdot \mathbf{e}_2^* \sum_j e^{i\mathbf{Q}\mathbf{r}_j}|0\rangle + \sum_n \frac{\langle f| \sum_j e^{-i\mathbf{K}_2\mathbf{r}_j}\mathbf{e}_2^* \cdot \mathbf{p}_j|n\rangle\langle n|e^{i\mathbf{K}_1\mathbf{r}_j}\mathbf{e}_1 \cdot \mathbf{p}_j|0\rangle}{\omega_1 - E_n} \right| \times \delta((\omega_1 - \omega_2) - E_f), \quad (1)$$

where $|0\rangle$ and $|f\rangle$ are the initial and final electronic state with energy $E_0 = 0$ and E_f, respectively. Eqn (1) includes both the

[a] *Physics Department and IRIS Adlershof, Humboldt-Universität zu Berlin, Zum Großen Windkanal 2, Berlin, Germany. E-mail: claudia.draxl@physik.hu-berlin.de; Fax: +49 30 2093 66362; Tel: +49 30 2093 66360*
[b] *LSI, Ecole Polytechnique, CNRS, CEA, Institut Polytechnique de Paris, F-91128 Palaiseau, France*
† Current address: Pritzker School of Molecular Engineering, University of Chicago, Chicago, IL 60637, USA.

non-resonant scattering (NRIXS), in which the momentum transfer $Q = K_1 - K_2$ appears explicitly, and the resonant scattering (RIXS). If the photon energy ω_1 is in resonance with the excitation energies E_n of the electronic system, the second, resonant term dominates and the non-resonant part can be neglected, leading to

$$\frac{\mathrm{d}^2\sigma}{\mathrm{d}\Omega_2\mathrm{d}\omega_2} = \alpha^4\left(\frac{\omega_2}{\omega_1}\right)\sum_f\left|\sum_n \frac{\langle f|\hat{T}^\dagger(\mathbf{e}_2)|n\rangle\langle n|\hat{T}(\mathbf{e}_1)|i\rangle}{\omega_1 - E_n + \mathrm{i}\eta}\right|^2 \times \delta(\omega_1 - \omega_2 - E_\mathrm{f}), \quad (2)$$

where we have introduced the transition operator $\hat{T}(e)$ in the dipole approximation, *i.e.*, $\hat{T}(\mathbf{e}) \approx \sum_j \mathbf{e}\cdot\mathbf{p}_j$. Microscopically, the resonant scattering process is as follows: The absorption of the initial X-ray photon with energy ω_1 excites a core electron into the conduction band, leaving a core hole behind. The intermediate system, after the excitation, is in an excited many-body state $|n\rangle$. The core hole can now be filled by a valence electron, which loses the energy ω_2 by emitting an X-ray photon. This process is known as direct RIXS. Alternatively, the presence of the core-hole and excited electron can lead to the formation of a secondary electron-hole pair in the intermediate state. The initially excited can then fill the core hole. This process is known as *indirect* RIXS.[2,32] Involving excited states beyond singlet excitations, its contribution is neglected in the following. We recall that indirect RIXS is mostly devoted to magnetic excitations, like magnon scattering.

In the final many-body state $|\mathrm{f}\rangle$, a hole is present in a valence state and an excited electron in a conduction state. While both the absorbed and emitted photon have energies in the X-ray region, the difference between them, the energy loss $\omega_1 - \omega_2$, is typically in the range of several eV. The final excited many-body state of the RIXS process corresponds to an excited state as typically created by optical absorption. The intricacy of the RIXS formalism, described in eqn (2), arises from the transitions between three many-body states, *i.e.*, $|0\rangle \rightarrow |n\rangle$ and $|n\rangle \rightarrow |\mathrm{f}\rangle$ and from the coherent summation over all possible intermediate and final many-body states. This inherent complexity of the microscopic RIXS process poses challenges for any theoretical description, as both the effects of electron-hole interaction, as well as the coherence of the RIXS process have to be included.

2.1 Independent-particle approximation to RIXS

It is instructive to discuss the RIXS process within the independent-particle approximation (IPA) before the scattering in the fully interactive system is considered. In the IPA, the many-body groundstate wavefunction is given by a single Slater determinant, and both the intermediate many-body state $|n\rangle$ and the final one $|\mathrm{f}\rangle$ are singlet excitations of the groundstate without any relaxation of the system. We know *a priori* that the intermediate states contain a core hole $\mu\mathbf{k}$ and an excited electron in a conduction state $c\mathbf{k}$, such that we can express them in second quantization as $|n\rangle = |c\mu\mathbf{k}\rangle = \hat{c}^\dagger_{c\mathbf{k}}\hat{c}_{\mu\mathbf{k}}|0\rangle$ with energy $E_n = \varepsilon_{c\mathbf{k}} - \varepsilon_{\mu\mathbf{k}}$. Furthermore, the final states contain an excited electron in a specific conduction state $c'\mathbf{k}'$ and a valence hole in the state $v\mathbf{k}$', such that $|\mathrm{f}\rangle = |c'\mathbf{k}'v\mathbf{k}'\rangle = \hat{c}^\dagger_{c'\mathbf{k}'}\hat{c}_{v\mathbf{k}'}|0\rangle$ and $E_\mathrm{f} = \varepsilon_{c'\mathbf{k}'} - \varepsilon_{v\mathbf{k}'}$. Then, eqn (2) becomes

$$\left.\frac{\mathrm{d}^2\sigma}{\mathrm{d}\Omega_2\mathrm{d}\omega_2}\right|_\mathrm{IP} = \alpha^4\left(\frac{\omega_2}{\omega_1}\right)\underbrace{\sum_{c'v\mathbf{k}'}}_{f}\left|\underbrace{\sum_{c\mu\mathbf{k}}}_{n}\frac{\langle c'v\mathbf{k}'|\hat{T}^\dagger(\mathbf{e}_2)|c\mu\mathbf{k}\rangle\langle c\mu\mathbf{k}|\hat{T}(\mathbf{e}_1)|0\rangle}{\omega_1 - (\varepsilon_{c\mathbf{k}} - \varepsilon_{\mu\mathbf{k}}) + \mathrm{i}\eta}\right|^2 \times \delta(\omega - (\varepsilon_{c'\mathbf{k}'} - \varepsilon_{v\mathbf{k}'})). \quad (3)$$

In second quantization, we express the transition operator as $\hat{T} = \sum_{mn}\sum_{\mathbf{k}}\mathbf{e}_1\cdot\mathbf{P}_{mn\mathbf{k}}\hat{c}^\dagger_{m\mathbf{k}}\hat{c}_{n\mathbf{k}}$, where $P_{mn\mathbf{k}} = \langle m\mathbf{k}|p|n\mathbf{k}\rangle$ are the momentum matrix elements. Inserting these operators in eqn (3) yields

$$\left.\frac{\mathrm{d}^2\sigma}{\mathrm{d}\Omega_2\mathrm{d}\omega_2}\right|_\mathrm{IP} = \sum_{c'v\mathbf{k}'}|\sum_{c\mu\mathbf{k}}\sum_{mn\mathbf{k}''}\sum_{pq\mathbf{k}'''}\left[\mathbf{e}_2^*\cdot\mathbf{P}_{mn\mathbf{k}''}\right] \times \frac{\langle c'v\mathbf{k}'|\hat{c}^\dagger_{m\mathbf{k}''}\hat{c}_{n\mathbf{k}''}|c\mu\mathbf{k}\rangle\langle c\mu\mathbf{k}|\hat{c}^\dagger_{p\mathbf{k}'''}\hat{c}_{q\mathbf{k}'''}|0\rangle}{\omega_1 - (\varepsilon_{c\mathbf{k}} - \varepsilon_{\mu\mathbf{k}}) + \mathrm{i}\eta}\left[\mathbf{P}_{pq\mathbf{k}'''}\cdot\mathbf{e}_1\right]|^2 \times \delta(\omega - (\varepsilon_{c'\mathbf{k}'} - \varepsilon_{v\mathbf{k}})). \quad (4)$$

We note that the summations over p and q in eqn (4) are not restricted to either core, valence, or conduction states. Restrictions to these indices can be inferred from the matrix elements of the creation and annihilation operators. We find that

$$\langle c\mu\mathbf{k}|\hat{c}^\dagger_{p\mathbf{k}'''}\hat{c}_{q\mathbf{k}'''}|0\rangle = \delta_{\mu q}\delta_{cp}\delta_{\mathbf{k}\mathbf{k}'''}. \quad (5)$$

The term $\langle c'v\mathbf{k}'|\hat{c}^\dagger_{m\mathbf{k}''}\hat{c}_{n\mathbf{k}''}|c\mu\mathbf{k}\rangle$ requires a more careful treatment. Applying Wick's theorem and restricting only to terms that correspond to the RIXS process, we obtain

$$\langle cv\mathbf{k}|\hat{c}^\dagger_{m\mathbf{k}''}\hat{c}_{n\mathbf{k}''}|c'\mu\mathbf{k}'\rangle = -\delta_{cc'}\delta_{\mu m}\delta_{vn}\delta_{\mathbf{k}\mathbf{k}'}\delta_{\mathbf{k}\mathbf{k}''}. \quad (6)$$

A more detailed derivation of eqn (6) is provided in the Appendix. Inserting eqn (5) and (6) into eqn (4) yields

$$\left.\frac{\mathrm{d}^2\sigma}{\mathrm{d}\Omega_2\mathrm{d}\omega_2}\right|_\mathrm{IP} = \alpha^4\left(\frac{\omega_2}{\omega_1}\right)\sum_{cv\mu\mathbf{k}}\left|\frac{\mathbf{e}_2^*\cdot\mathbf{P}_{\mu v\mathbf{k}}\mathbf{P}_{c\mu\mathbf{k}}\cdot\mathbf{e}_1}{\omega_1 - (\varepsilon_{c\mathbf{k}} - \varepsilon_{\mu\mathbf{k}}) + i\eta}\right|^2 \times \delta(\omega - (\varepsilon_{c\mathbf{k}} - \varepsilon_{v\mathbf{k}})) = -\frac{\alpha^4}{\pi}\left(\frac{\omega_2}{\omega_1}\right)\mathrm{Im}\sum_{cv\mathbf{k}}\frac{\left|\sum_\mu \frac{\mathbf{e}_2^*\cdot\mathbf{P}_{\mu v\mathbf{k}}\mathbf{P}_{c\mu\mathbf{k}}\cdot\mathbf{e}_1}{\omega_1 - (\varepsilon_{c\mathbf{k}} - \varepsilon_{\mu\mathbf{k}}) + i\eta}\right|^2}{\omega - (\varepsilon_{c\mathbf{k}} - \varepsilon_{v\mathbf{k}}) + i\eta}. \quad (7)$$

This equation has been widely applied to calculate the RIXS cross section in solids.[33–38]

2.2 RIXS beyond the independent-particle approximation

The neglected electron-hole interaction is the reason for the poor performance of the IPA for optical and X-ray excitation spectra in crystalline semiconductors and insulators. A more accurate approach is provided by many-body perturbation theory based on solutions of the BSE.[10,39,40] This approach is

now the state of the art to determine optical[9,11,39,41–43] and X-ray absorption spectra[22,25,29,44–55] in solids. In the following, we derive an analytical expression for RIXS that takes the electron-hole interaction into account.

Following ref. 14 and 17, we define an intermediate many-body state as

$$|Y(\omega_1)\rangle = \sum_n \frac{|n\rangle\langle n|}{\omega_1 - E_n}\hat{T}(\mathbf{e}_1)|0\rangle. \tag{8}$$

Similar intermediate states have been defined as *response vectors* in the context of non-linear spectroscopy in molecular systems.[56,57] Inserting these intermediate states into eqn (2), the RIXS cross section becomes

$$\begin{aligned}\frac{\mathrm{d}^2\sigma}{\mathrm{d}\Omega_2\mathrm{d}\omega_2} &= \alpha^4\left(\frac{\omega_2}{\omega_1}\right)\sum_f |\langle f|\hat{T}^\dagger(\mathbf{e}_2)|Y(\omega_1)\rangle|^2\delta(\omega - E_f)\\ &= \alpha^4\left(\frac{\omega_2}{\omega_1}\right)\sum_f \langle Y(\omega_1)|\hat{T}(\mathbf{e}_2)|f\rangle\langle f|\hat{T}^\dagger(\mathbf{e}_2)|Y(\omega_1)\rangle\delta(\omega - E_f).\end{aligned} \tag{9}$$

The intermediate states $|Y(\omega_1)\rangle$ contain the information about all possible excitation processes and can be understood as the excited many-body states produced by the absorption of a photon with energy ω_1. Inserting a finite broadening η for the excited many-body states, the cross section becomes

$$\frac{\mathrm{d}^2\sigma}{\mathrm{d}\Omega_2\mathrm{d}\omega_2} = \alpha^4\left(\frac{\omega_2}{\omega_1}\right)\mathrm{Im}\sum_f \frac{\langle Y(\omega_1)|\hat{T}(\mathbf{e}_2)|f\rangle\langle f|\hat{T}^\dagger(\mathbf{e}_2)|Y(\omega_1)\rangle}{\omega - E_f + \mathrm{i}\eta}. \tag{10}$$

Within the Tamm–Dancoff approximation, we assume that both the intermediate and final states are linear combinations of singlet excitations of the groundstate. We can thus infer

$$1 \approx \sum_{i\mathbf{k}}\sum_{j\mathbf{k}'} \hat{c}^\dagger_{j\mathbf{k}'}\hat{c}_{i\mathbf{k}}|0\rangle\langle 0|\hat{c}^\dagger_{i\mathbf{k}}\hat{c}_{j\mathbf{k}'}. \tag{11}$$

While this approximation has been found to yield good results for the excited states probed in both optical and X-ray absorption spectroscopy of solids,[29,30] it explicitly limits our approach to *direct* RIXS, as the intermediate states in *indirect* RIXS contain two electron-hole pairs and therefore can not be expressed as a linear combination of singlet excitations of the groundstate. Inserting eqn (11) into eqn (8) yields

$$\begin{aligned}|Y(\omega_1)\rangle &= \sum_n\sum_{c\mu\mathbf{k}}\sum_{c'\mu'\mathbf{k}'}\hat{c}^\dagger_{c\mathbf{k}}\hat{c}_{\mu\mathbf{k}}|0\rangle\frac{\langle 0|\hat{c}^\dagger_{\mu\mathbf{k}}\hat{c}_{c\mathbf{k}}|n\rangle\langle n|\hat{c}^\dagger_{c'\mathbf{k}'}\hat{c}_{\mu'\mathbf{k}'}|0\rangle}{\omega_1 - E_n}\left[\mathbf{e}_1\cdot\mathbf{P}_{c'\mu'\mathbf{k}'}\right]\\ &= \sum_{c\mu\mathbf{k}}\sum_{c'\mu'\mathbf{k}'}\hat{c}^\dagger_{c\mathbf{k}}\hat{c}_{\mu\mathbf{k}}|0\rangle\chi_{c\mu\mathbf{k},c'\mu'\mathbf{k}'}(\omega_1)\left[\mathbf{e}_1\cdot\mathbf{P}_{c'\mu'\mathbf{k}'}\right],\end{aligned} \tag{12}$$

where we have made use of the Lehmann representation of the polarizability $\chi(\omega)$. We can now evaluate the expectation value of the intermediate state

$$\begin{aligned}&\langle Y(\omega_1)|\hat{c}^\dagger_{j\mathbf{k}''}\hat{c}_{i\mathbf{k}''}\hat{c}^\dagger_{c'''\mathbf{k}'''}\hat{c}^\dagger_{v'''\mathbf{k}'''}|0\rangle\\ &= -\sum_{c\mu\mathbf{k}}\sum_{c'\mu'\mathbf{k}'}\chi^*_{c\mu\mathbf{k},c'\mu'\mathbf{k}'}(\omega_1)\left[\mathbf{e}_1\cdot\mathbf{P}_{c'\mu'\mathbf{k}'}\right]^*\delta_{cc'''}\delta_{v'''j}\delta_{\mu i}\delta_{\mathbf{k}\mathbf{k}'''}\delta_{\mathbf{k}\mathbf{k}''}\end{aligned} \tag{13}$$

where we have used eqn (6). This eventually yields the double-differential cross section as

$$\begin{aligned}\frac{\mathrm{d}^2\sigma}{\mathrm{d}\Omega_2\mathrm{d}\omega_2} &= \alpha^4\left(\frac{\omega_2}{\omega_1}\right)\mathrm{Im}\sum_{c,c',c'',c'''}\sum_{\mu,\mu',\mu'',\mu'''}\sum_{v,v'}\sum_{\mathbf{k}\mathbf{k}'\mathbf{k}''\mathbf{k}'''}\\ &\times\left[\left[\mathbf{e}_2^*\cdot\mathbf{P}_{\mu v\mathbf{k}}\right]\chi_{c\mu\mathbf{k},c'\mu'\mathbf{k}'}(\omega_1)\left[\mathbf{e}_1\cdot\mathbf{P}_{c'\mu'\mathbf{k}'}\right]\right]^*\\ &\times\chi_{cv\mathbf{k},c''v'\mathbf{k}''}(\omega)\left[\left[\mathbf{e}_2^*\cdot\mathbf{P}_{\mu''v'\mathbf{k}''}\right]\chi_{c''\mu''\mathbf{k}'',c'''\mu'''\mathbf{k}''}(\omega_1)\left[\mathbf{e}_1\cdot\mathbf{P}_{c'''\mu'''\mathbf{k}''}\right]\right].\end{aligned} \tag{14}$$

Eqn (14) represents a main result of this paper: The RIXS cross section is expressed solely in terms of the polarizability χ. The polarizability is evaluated twice, once at the X-ray excitation energy ω_1, and once at the energy loss $\omega = \omega_1 - \omega_2$. The cumbersome summations over all intermediate and final many-body states are thus included in the polarizability, and eqn (14) avoids any explicit summations over many-body states.

2.3 Many-body perturbation theory applied to RIXS

Within MBPT, the polarizability is given by

$$\chi_{ij\mathbf{k},i'j'\mathbf{k}'}(\omega) = \sum_\lambda \frac{\left[X_{ij\mathbf{k},\lambda}\right]^* X_{i'j'\mathbf{k}',\lambda}}{\omega - E^\lambda + \mathrm{i}\eta}, \tag{15}$$

where $X_{ij\mathbf{k},\lambda}$ and E^λ are the eigenstates and -values of the BSE equation

$$H^{\mathrm{BSE}}X_\lambda = E^\lambda X_\lambda, \tag{16}$$

where the Hamiltonian is given by

$$H^{\mathrm{BSE}} = \Delta E^{\mathrm{IP}} + 2V - W. \tag{17}$$

Here, ΔE^{IP} are the single-particle energy differences which are taken from DFT Kohn-Sham calculations and are corrected by a scissors operator. The corresponding values for conduction states and core states are chosen such to simulate the zero-order polarizability in the BSE calculations.[59] V are the matrix elements of the bare electron-hole exchange, and W those of the statically screened direct interaction.

Inserting eqn (15) into eqn (14) allows for a significant simplification of the RIXS cross section. We first consider the last bracket of eqn (14) and express it as

$$\begin{aligned}&\sum_{c'''\mu'''\mathbf{k}'''}\sum_{\mu''}\left[\mathbf{e}_2^*\cdot\mathbf{P}_{\mu''v'\mathbf{k}''}\right]\chi_{c''\mu''\mathbf{k}'',c'''\mu'''\mathbf{k}'''}(\omega_1)\left[\mathbf{e}_1\cdot\mathbf{P}_{c'''\mu'''\mathbf{k}'''}\right]\\ &= \sum_{\mu''}\sum_{\lambda_c}\left[\mathbf{e}_2^*\cdot\mathbf{P}_{\mu''v'\mathbf{k}''}\right]\frac{\left[X_{c''\mu''\mathbf{k}'',\lambda_c}\right]^* t^{(1)}_{\lambda_c}}{\omega_1 - E^{\lambda_c} + \mathrm{i}\eta},\end{aligned} \tag{18}$$

where $X_{c''\mu''\mathbf{k}''}$ and E^{λ_c} are the eigenvectors and -values of the core-level BSE, respectively. We define the core-excitation

oscillator strength $t^{(1)}_{\lambda_c}$ as

$$t^{(1)}_{\lambda_c} = \sum_{c'''\mu'''\mathbf{k}'''} X_{c'''\mu'''\mathbf{k}''',\lambda_c} \left[\mathbf{e}_1 \cdot \mathbf{P}_{c'''\mu'''\mathbf{k}'''}\right] \tag{19}$$

and the excitation pathway $t^{(2)}_{\lambda_o,\lambda_c}$ as

$$t^{(2)}_{\lambda_o,\lambda_c} = \sum_{c\nu\mathbf{k}} \sum_{\mu} X_{c\nu\mathbf{k},\lambda_o} \left[\mathbf{e}_2^* \cdot \mathbf{P}_{\mu\nu\mathbf{k}}\right] \left[X_{c\mu\mathbf{k},\lambda_c}\right]^*, \tag{20}$$

where $X_{c\nu\mathbf{k},\lambda_o}$ and E^{λ_o} are the eigenvectors and -values of the BSE Hamiltonian of the valence-conduction transitions, respectively. Here, we discern the index of the valence-conduction excitations, λ_o, from the index λ_c of the core-conduction ones.

Inserting eqn (18) and (20) into eqn (14) yields

$$\frac{\mathrm{d}^2\sigma}{\mathrm{d}\Omega_2 \mathrm{d}\omega_2} = \alpha^4 \left(\frac{\omega_2}{\omega_1}\right) \mathrm{Im} \sum_{\lambda_o} \frac{\left|\sum_{\lambda_c} \frac{t^{(2)}_{\lambda_o,\lambda_c} t^{(1)}_{\lambda_c}}{\omega_1 - E^{\lambda_c} + \mathrm{i}\eta}\right|^2}{(\omega_1 - \omega_2) - E^{\lambda_o} + \mathrm{i}\eta}. \tag{21}$$

Finally, we define the RIXS oscillator strength $t^{(3)}_{\lambda}(\omega_1)$ as

$$t^{(3)}_{\lambda_o}(\omega_1) = \sum_{\lambda_c} \frac{t^{(2)}_{\lambda_o,\lambda_c} t^{(1)}_{\lambda_c}}{\omega_1 - E^{\lambda_c} + \mathrm{i}\eta}. \tag{22}$$

Using the definition of the oscillator strength $t^{(1)}_{\lambda_c}$ in eqn (19) and the excitation pathway $t^{(2)}_{\lambda_o,\lambda_c}$ in eqn (20), allows for the compact expression of the RIXS cross section as

$$\frac{\mathrm{d}^2\sigma}{\mathrm{d}\Omega_2 \mathrm{d}\omega_2} = \alpha^4 \left(\frac{\omega_2}{\omega_1}\right) \mathrm{Im} \sum_{\lambda_o} \frac{|t^{(3)}_{\lambda_o}(\omega_1)|^2}{(\omega_1 - \omega_2) - E^{\lambda_o} + i\eta} \tag{23}$$

which closely resembles the BSE expression for optical and X-ray absorption spectra. The cross section depends explicitly on the energy loss $\omega = \omega_1 - \omega_2$, while its dependence on the excitation energy is contained in the oscillator strength $t^{(3)}_{\lambda_o}(\omega_1)$. It has poles in the energy loss at the optical excitation energies E^{λ_o} of the system, independent of the excitation energy, while the oscillator strength of each of these excitations depends on it. The oscillator strength defined in eqn (22), gives further insight into the many-body processes that occur in RIXS. The rate of the initial X-ray absorption event is given by $t^{(1)}_{\lambda_c}$, combined with the energy conservation rule (the denominator $\omega_1 - E^{\lambda_c} + i\eta$ in eqn (22)). The absorption leads to an intermediate core-excited state, characterized by the excitation index λ_c. The final RIXS spectrum is then given by the rate of the absorption combined with the pathway $t^{(2)}_{\lambda_o,\lambda_c}$ that describes the many-body transition $|\lambda_c\rangle \rightarrow |\lambda_o\rangle$. These pathways are far from obvious, as the mixing between $t^{(1)}_{\lambda_c}$ and $t^{(2)}_{\lambda_o,\lambda_o}$ can develop in destructive or constructive interference, attesting the many-body character of such process.

With eqn (23), we have derived a compact analytical expression for the double-differential RIXS cross section with only two assumptions: First, we presume in eqn (11) that the intermediate and final states are singlet excitations. While this assumption limits our approach to direct RIXS, it is consistent with the Tamm–Dancoff approximation in the BSE formalism. Second, we assume that the latter yield accurate core and valence excited states. Therefore, these approximations are interconnected. For systems, such as diamond and Ga_2O_3 studied here, where BSE yields accurate absorption spectra, our approach yields accurate RIXS spectra as well. For highly correlated states, BSE results may strongly depend on the starting point, *i.e.*, the underlying one-particle states. It might happen, for instance, that semilocal DFT leads to a poor representation of the system. In this case, even the BSE result will be poor. This is neither a problem of BSE nor of the RIXS formulation. Here, one-particle wave functions coming from hybrid functionals, or self-consistent COHSEX or GW will be required, as shown for copper and vanadium oxides.[60,61] Such calculations are, however, not standard to date as they are numerically very involved. All in all, the RIXS formulation provided here, is very general and fully *ab initio*, and it applies to a large variety of systems.

3 Implementation

The implementation of eqn (23) requires explicit access to the BSE eigenvectors $X_{c\nu\mathbf{k}\lambda_o}$ both in terms of valence-conduction transitions $X_{c\mu\mathbf{k}\lambda_c}$ as well as core-conduction transitions, while cross terms of the form $X_{v\mu\mathbf{k}\lambda}$ are not needed. Thus, the calculation of the RIXS cross section can be separated into three independent calculations, one for the core-conduction, one for the valence-conduction excitations, and finally a convolution step to obtain the RIXS cross section. Overall, momentum matrix elements $P_{c\mu\mathbf{k}}$ between core and conduction states and $P_{\mu\nu\mathbf{k}}$ between valence and core states determine the excitation and de-excitation process, respectively. The coherence between core and valence excitations in the RIXS process is apparent in eqn (20) from the summation over $\mathbf{k}$. (For this reason, core and valence excitations are calculated on the same $\{\mathbf{k}\}$-grid.) Coherence occurs, since the absorption and emission processes conserve the crystal momentum $\mathbf{k}$.[1]

For the specific implementation, we make use of the core-conduction and valence-conduction BSE eigenvectors and corresponding matrix elements obtained from the all-electron package `exciting`.[28–30] The output of the two BSE calculations is evaluated by the BRIXS (BSE for RIXS) code.[62,63] In this step, the oscillator strength $t^{(1)}$ of the core excitation and the excitation pathways $t^{(2)}$ are determined. From these intermediate quantities, the RIXS oscillator strength $t^{(3)}(\omega_1)$ is generated for a list of excitation energies ω_1 defined by the user. Execution of BRIXS requires only a minimal number of input parameters: Besides $\{\omega_1\}$, the number of core-conduction ($N_{\lambda c}$) and valence-conduction excitations ($N_{\lambda o}$), the lifetime broadening (η), and the polarization vector of the X-ray beam (e_1) are required. A detailed description of the implementation is provided in ref. 64.

4 Results

4.1 Electron-hole correlation in the RIXS of diamond

To demonstrate the importance of electron-hole correlation in RIXS, we study the carbon K edge in diamond. Both optical

absorption[12,58,66–68] and core excitations[65,69,70] have been investigated intensively before. RIXS measurements[33,65] and calculations[14,17] are also available for this edge. As such, this material acts as a good example to demonstrate our approach and benchmark the resulting spectra.

In a first step, the optical and core spectra are calculated from the solution of the BSE, as shown in Fig. 1, both in excellent agreement with experiment. In addition, we show the results obtained within the independent-particle approximation (IPA). They are blue-shifted relative to experiment, as electron-hole attraction is not included. Also the spectral shape of the core spectra disagrees with the experimental one, as it misses the peak at the absorption onset and shows too much spectral weight at high energies.

From the BSE spectra, we determine the RIXS specrtra shown in Fig. 1. Following eqn (21) and (22), it comes natural to display the RIXS double-differential cross section $d^2\sigma/d\Omega_2 d\omega_2$ as a function of the excitation energy ω_1 and the energy loss $\omega = \omega_1 - \omega_2$. For excitation energies below the core absorption edge, *i.e.*, at approximately 290 eV (see Fig. 2, right), the intensity is negligible, since the excitation energy is not in resonance with any carbon 1*s* excitation. Once the excitation energy reaches resonance with the absorption edge, the RIXS cross section increases considerably. The emission occurs over a wide range of the energy loss up to around 20 eV, but is strongest at low emission at the onset of optical absorption (compare Fig. 1, top). With increasing excitation energy, the emission reduces due to the reduced rate of absorption beyond the onset. Furthermore, the emission at low energy loss vanishes as the excitation energy increases. At a value of about 295 eV (300 eV), no emission with an energy loss below approximately 12 eV (20 eV) is observed. Due to this linear dispersion of the energy loss with the excitation energy, the emission energies stay more or less constant, as can be seen in Fig. 2, where the RIXS cross section is shown as a function of the emission energy for selected excitation energies.

In Fig. 2, we also show the RIXS cross section obtained within the IPA, following eqn (7). Overall, the IPA spectra exhibit lower emission energies due to the overestimation of the excitation energies in the optical absorption (see Fig. 1). Especially for lower excitation energies, there are significant deviations. The intensity at higher emission energies is underestimated, and the spectra are too broad. Both features are due to the neglect of electron-hole interaction which increases the intensity at low energies, *i.e.*, leads to a sharper absorption onsets. This effect is especially pronounced for the core excitations. At higher excitation energies, the discrepancy between IPA and BSE results decreases. While IPA reproduces the spectral shape correctly, the spectrum is still blue-shifted. Our BSE results are in excellent agreement with experiment for all excitations energies, both in relative position and spectral shape.

4.2 Atomic coherence in the RIXS of Ga_2O_3

Now, we like to showcase the importance of atomic coherence on RIXS spectra. Considering the coherent sum over atomic excitations in eqn (21), interference terms appear when the

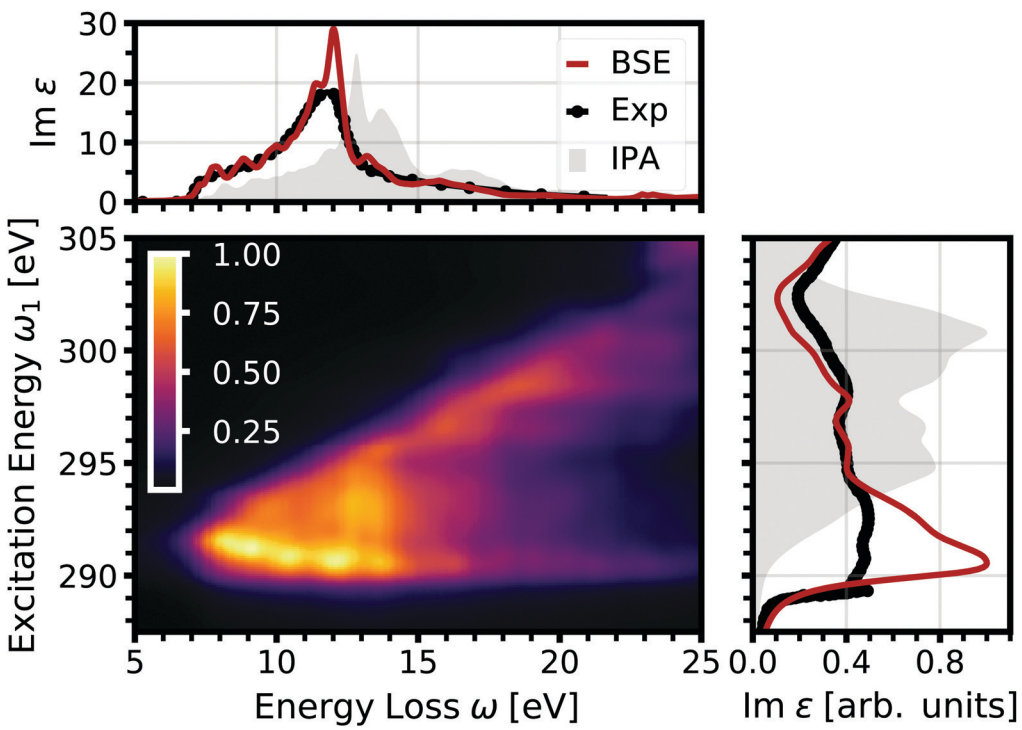

Fig. 1 Normalized double-differential RIXS cross section of the carbon K edge in diamond as a function of excitation energy and energy loss (center). On the top, the optical absorption spectrum obtained from BSE (red) and the IPA (gray) is shown, compared to the experimental spectrum (black) from ref. 58. On the right, the corresponding core excitation is depicted.

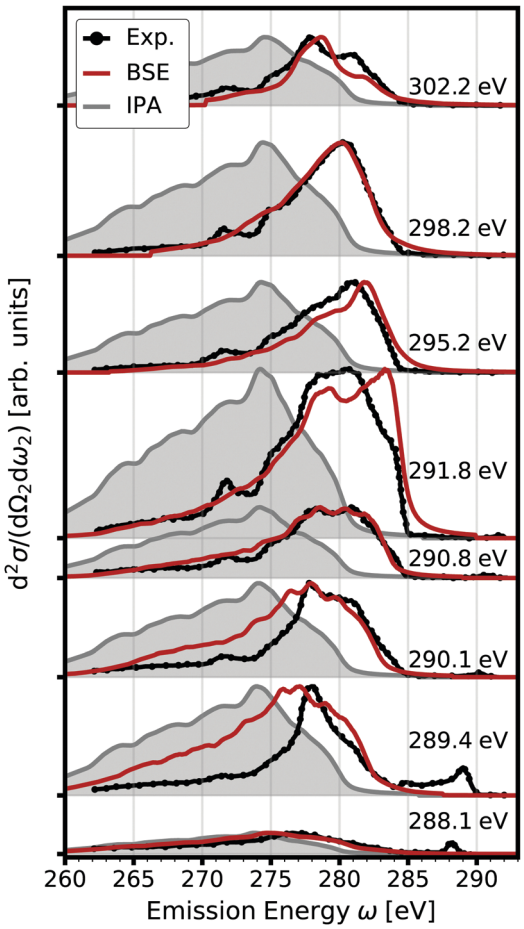

Fig. 2 Double differential RIXS cross section (red) accounting for electron-hole interaction. The spectra calculated for several excitation energies are offset for clarity. Experimental data from ref. 65 are shown in black, the IPA results in gray.

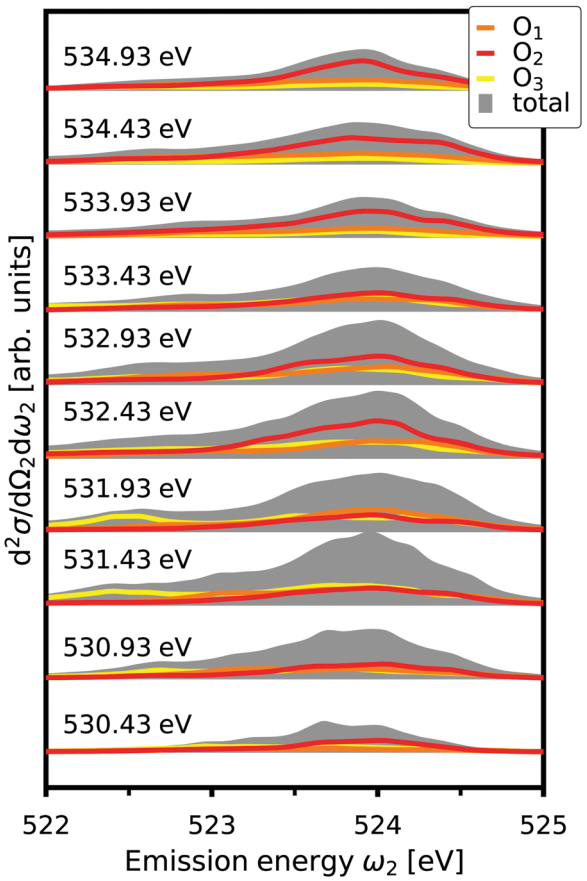

Fig. 3 Total O K edge RIXS in β-Ga_2O_3 as a function of emission energy, ω_2, for selected excitation energies, together with the contributions from O_1,O_2, and O_3. The spectra are offset for clarity.

crystal contains inequivalent atomic positions, *i.e.*,

$$\frac{d^2\sigma}{d\Omega_2 d\omega_2} = \sum_a^{N_{atoms}} M_a{}^2 \frac{d^2\sigma_a}{d\Omega_2 d\omega_2} + \frac{d^2\sigma_{interf}}{d\Omega_2 d\omega_2}, \qquad (24)$$

where $d^2\sigma_a/d\Omega_2 d\omega_2$ is the RIXS cross section for the inequivalent atom a with multiplicity M_a and $d^2\sigma_{interf}/d\Omega_2 d\omega_2$ is the interference term. Mathematically, the interference term originates from the square modulus of $t_\lambda^{(3)}(\omega_1)$ in eqn (21) that contains the sum of the core excitations on all atoms in the unit cell. The O K edge in the monoclinic β phase of Ga_2O_3 serves as an example. The unit cell contains three inequivalent oxygen sites denoted O_1,O_2, and O_3, all of them with multiplicity 1. Fig. 3 shows that the RIXS spectrum shows pronounced fluorescence behavior,[71,72] *i.e.*, significant features occur at basically constant emission energies. The contributions of all oxygen atoms are nearly identical for excitation energies below 532 eV. Above that, the contribution of O_2 dominates the spectrum. For a quantitative analysis, we define relative atomic contributions by integrating the atomic RIXS spectra over the emission energies ω_2 and normalizing with respect to the total spectrum. The result, shown in Fig. 4, demonstrates that the relative atomic contributions vary between 20 and 50%, depending on the excitation energy, and that none of the contributions can be neglected even if one of them – here O_2 – dominates. The interference term contributes up to 15% of the total RIXS spectrum, yet decreasing quickly as the excitation energy increases beyond the absorption onset. At higher excitation energies, it only contributes 5–7%. The importance of interference at the absorption onset indicates that it originates from electronic correlation.

5 Conclusions

We have derived a compact analytical expression for the RIXS cross section within many-body perturbation theory. This expression retains the intuitive interpretation of the RIXS process as a coherent absorption-emission process, while including the effects of electron-hole correlation, which are paramount for an accurate description of excitations in semiconductors and insulators. Our implementation in an all-electron BSE framework, *i.e.*, the `exciting` package, making use of BSE eigenstates for core and valence excitations, introduces only small computational overhead compared to valence and core BSE calculations. For the example of the carbon K edge RIXS in diamond, we demonstrate that our approach

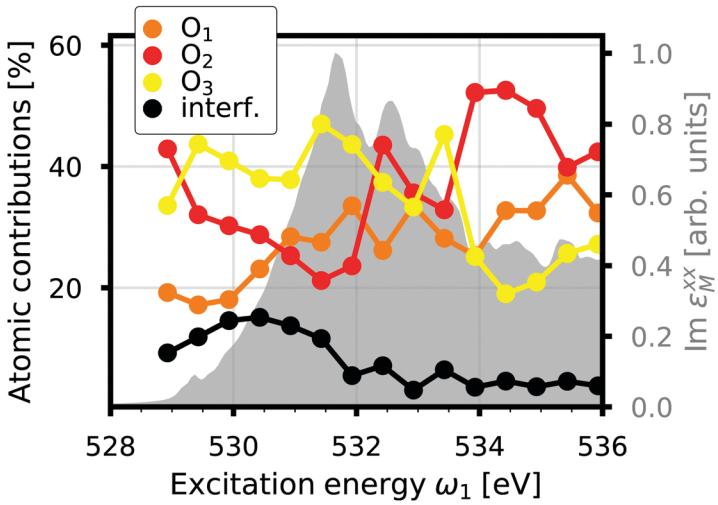

Fig. 4 Interference contribution to the O K edge RIXS of β-Ga_2O_3 as a function of excitation energy compared to the atomic contributions and the normalized total spectrum (gray).

yields spectra in excellent agreement with available experimental spectra. We furthermore show that electron-hole correlations not only shift spectral features in energy but also affect their shape, especially in excitations at the absorption edge. The influence of atomic coherence is exemplified with the oxygen K edge in β-Ga_2O_3, where it turns out non-negligible, especially close to the absorption onset.

Author contributions

All authors have devised the project. FS and CV derived the RIXS formalism, CV implemented it in the all-electron package `exciting` and carried out the calculations. All authors contributed to the writing of the manuscript.

Conflicts of interest

There are no conflicts to declare.

Appendix. Derivation of matrix elements

In the following, we provide the derivation of eqn (6). We initially employ Wick's theorem[73] to evaluate the expectation value of the product of three pairs of annihilation and creation operators, *i.e.*,

$$\begin{aligned}\langle c\nu\mathbf{k}|\hat{c}^\dagger_{m\mathbf{k}''}\hat{c}_{n\mathbf{k}''}|c'\mu\mathbf{k}'\rangle &= \langle 0|\left[\hat{c}^\dagger_{\nu\mathbf{k}}\hat{c}_{c\mathbf{k}}\right]\left[\hat{c}^\dagger_{m\mathbf{k}''}\hat{c}_{n\mathbf{k}''}\right]\left[\hat{c}^\dagger_{c'\mathbf{k}'}\hat{c}_{\mu\mathbf{k}'}\right]|0\rangle \\ &= \delta_{\nu\mu}\delta_{c'n}\delta_{cm}\delta_{\mathbf{k}\mathbf{k}'}\delta_{\mathbf{k}\mathbf{k}''} \\ &\quad + \delta_{cc'}\delta_{mn}\delta_{\nu\mu}\delta_{\mathbf{k}\mathbf{k}'}\delta_{\mathbf{k}\mathbf{k}''} \\ &\quad - \delta_{cc'}\delta_{\mu m}\delta_{\nu n}\delta_{\mathbf{k}\mathbf{k}'}\delta_{\mathbf{k}\mathbf{k}''}.\end{aligned} \tag{25}$$

Each of the three contributions correspond to different processes in the DDCS. To analyze them, we insert eqn (25) into eqn (7). Ignoring cross-terms, this yields the following expressions:

$$\left.\frac{\mathrm{d}^2\sigma}{\mathrm{d}\Omega_2\mathrm{d}\omega_2}\right|_{\mathrm{IP}} = \alpha^4\left(\frac{\omega_2}{\omega_1}\right)\begin{cases}\sum_{c'\mu\mathbf{k}}\left|\sum_c \frac{\mathbf{e}_2^*\cdot\mathbf{P}_{c'c\mathbf{k}}\mathbf{P}_{c\mu\mathbf{k}}\cdot\mathbf{e}_1}{\omega_1-(\varepsilon_{c\mathbf{k}}-\varepsilon_{\mu\mathbf{k}})+\mathrm{i}\eta}\right|^2 & \text{(a)} \\ \quad\times\delta(\omega-(\varepsilon_{c'\mathbf{k}}-\varepsilon_{\mu\mathbf{k}})) & \\ +\sum_{c\mu\mathbf{k}}\left|\sum_m \frac{\mathbf{e}_2^*\cdot\mathbf{P}_{mm\mathbf{k}}\mathbf{P}_{c\mu\mathbf{k}}\cdot\mathbf{e}_1}{\omega_1-(\varepsilon_{c\mathbf{k}}-\varepsilon_{\mu\mathbf{k}})+\mathrm{i}\eta}\right|^2 & \text{(b)} \\ \quad\times\delta(\omega-(\varepsilon_{c\mathbf{k}}-\varepsilon_{\mu\mathbf{k}})) & \\ +\sum_{c\nu\mathbf{k}}\left|\sum_\mu \frac{\mathbf{e}_2^*\cdot\mathbf{P}_{\mu\nu\mathbf{k}}\mathbf{P}_{c\mu\mathbf{k}}\cdot\mathbf{e}_1}{\omega_1-(\varepsilon_{c\mathbf{k}}-\varepsilon_{\mu\mathbf{k}})+\mathrm{i}\eta}\right|^2 & \text{(c)} \\ \quad\times\delta(\omega-(\varepsilon_{c\mathbf{k}}-\varepsilon_{\nu\mathbf{k}})) & \end{cases} \tag{26}$$

An intuitive interpretation of the three terms is obtained by considering their poles: Term (a) has poles at the excitation energies $\omega_1 = \varepsilon_{c\mathbf{k}} - \varepsilon_{\mu\mathbf{k}}$, where a core state $\mu\mathbf{k}$ is excited into a conduction state $c\mathbf{k}$. Poles in the emission energy occur at $\omega_2 = \varepsilon_{c'\mathbf{k}} - \varepsilon_{c\mathbf{k}}$ where the excited electron transitions to another conduction state $c'\mathbf{k}$. Thus, the final state of this scattering process contains a core hole at $\mu\mathbf{k}$ and an excited electron in $c'\mathbf{k}$. As such, this scattering process does not correspond to the RIXS process.

Term (b) does not describe a resonant scattering process, as the emission energy ω_2 vanishes (corresponding to transitions $m\mathbf{k} \to m\mathbf{k}$). However, for each state, the momentum matrix element $P_{mm\mathbf{k}} = 0$. Thus, term (b) does not contribute to the DDCS.

Finally, term (c) corresponds to the RIXS process: Poles occur at excitation energies $\omega_1 = \varepsilon_{c\mathbf{k}} - \varepsilon_{\mu\mathbf{k}}$ and at emission energies $\omega_2 = \varepsilon_{\nu\mathbf{k}} - \varepsilon_{\mu\mathbf{k}}$. Thus, the scattering consists of an excitation $\mu\mathbf{k} \to c\mathbf{k}$ and a subsequent de-excitation $\nu\mathbf{k} \to \mu\mathbf{k}$. The final state contains a valence hole $\nu\mathbf{k}$ and an excited electron $c\mathbf{k}$.

Overall, as long we only consider RIXS, we can neglect terms (a) and (b), and we arrive at eqn (14). The analysis also justifies why the cross terms between the terms (a), (b), and (c) can be neglected. The different terms have poles in vastly different energy regions, thus making cross terms small.

Numerical parameters

Carbon K edge in diamond

The electronic structure is determined from DFT-PBE calculations within the `exciting` code. All calculations are performed for the experimental lattice parameter of 6.746 a_0. The reciprocal space is sampled with a $9 \times 9 \times 9$ **k**-grid, and we include basis functions up to a cut-off of $R_{MT}^{max} \cdot |G + q|_{max} = 8$. To correct the electronic structure, we apply a scissors operator $\Delta\omega$ = 1.9 eV, such to reproduce the measured indirect band gap of 5.48 eV.[74] Another scissors operator of 22 eV is employed to correct the position of the 1*s* level.

Optical BSE spectra are calculated on a $13 \times 13 \times 13$ **k**-grid, and local-field effects are included up to a cut-off $|G + q|_{max} = 3.5\ a_0^{-1}$. The calculations include all 4 valence bands and 10 conduction bands. 100 conduction bands are included in the random-phase approximation (RPA) calculation to obtain the screened Coulomb potential. The carbon K edge BSE is performed on the same **k**-grid. The cut-off for local-field is chosen $|G + q|_{max} = 5.5\ a_0^{-1}$ such to provide a precise description of the more localized excitations. 40 unoccupied are included in the BSE calculation. For the BRIXS calculation, the 8.000 lowest-energy valence and 20 000 carbon 1s excitations are taken into account.

Input and relevant output files of the electronic-structure and BSE calculations can be downloaded from the NOMAD Repository[75,76] under the DOI provided in ref. 77.

O K edge in β-Ga_2O_3

Calculations for β-Ga_2O_3 are performed using the experimental lattice parameters a = 12.233 Å, b = 3.038 Å, c = 5.807 Å, and β = 103.82°.[78] The electronic structure is determined on a $8 \times 8 \times 8$ **k**-grid using basis functions up to a cut-off of $R_{MT}^{max} \cdot |G + q|_{max} = 8$. Our calculations with the PBEsol functional[79] yield a Kohn-Sham gap of 2.89 eV. To match the experimental fundamental gap of of 5.72 eV,[80] we apply a scissors operator of $\Delta\omega$ = 2.6 eV. A scissors shift of $\Delta\omega_2$ = 24.93 eV is applied to correct the position of the oxygen 1*s* state such to align the calculated O K edge XAS with the experimental one.[81]

The optical BSE spectra are obtained from calculations on a $10 \times 10 \times 10$ **k**-grid with a cut-off $|G + q|_{max} = 1.1\ a_0^{-1}$ for local-field effects. The 10 highest valence bands and 10 lowest conduction bands form the transition space. 30 conduction bands are used in the RPA calculation of the screened Coulomb potential.

The BSE calculation of the oxygen K edge are performed on the same **k**-grid and using the identical screened Coulomb potential as for the optical spectra. 20 conduction bands are used to form the transition space.

Input and relevant output files of the electronic-structure and BSE calculations can be downloaded from the NOMAD Repository[75,76] under the DOI provided in ref. 82.

Acknowledgements

This work was supported by the project GraFOx, a Leibniz ScienceCampus, partially funded by the Leibniz Association. FS thanks the French Agence Nationale de la Recherche (ANR) for financial support (grant No. ANR-19-CE30-0011).

Notes and references

1 A. Kotani and S. Shin, *Rev. Mod. Phys.*, 2001, **73**, 203–246.
2 L. J.-P. Ament, M. van Veenendaal, T. P. Devereaux, J. P. Hill and J. van den Brink, *Rev. Mod. Phys.*, 2011, **83**, 705–767.
3 A. Cesar, F. Gelmukhanov, Y. Luo, H. Ågren, P. Skytt, P. Glans, J. Guo, K. Gunnelin and J. Nordgren, *J. Chem. Phys.*, 1997, **106**, 3439–3456.
4 F. Hennies, S. Polyutov, I. Minkov, A. Pietzsch, M. Nagasono, H. Ågren, L. Triguero, M.-N. Piancastelli, W. Wurth, F. Gelmukhanov and A. Föhlisch, *Phys. Rev. A: At., Mol., Opt. Phys.*, 2007, **76**, 032505.
5 I. Josefsson, K. Kunnus, S. Schreck, A. Föhlisch, F. de Groot, P. Wernet and M. Odelius, *J. Phys. Chem. Lett.*, 2012, **3**, 3565–3570.
6 G. Ghiringhelli, M. Matsubara, C. Dallera, F. Fracassi, R. Gusmeroli, A. Piazzalunga, A. Tagliaferri, N. B. Brookes, A. Kotani and L. Braicovich, *J. Phys.: Condens. Matter*, 2005, **17**, 5397–5412.
7 R.-P. Wang, B. Liu, R. J. Green, M. U. Delgado-Jaime, M. Ghiasi, T. Schmitt, M. M. van Schooneveld and F. M.-F. de Groot, *J. Phys. Chem. C*, 2017, **121**, 24919–24928.
8 L. Hedin, *Phys. Rev.*, 1965, **139**, A796–A823.
9 M. S. Hybertsen and S. G. Louie, *Phys. Rev. Lett.*, 1985, **55**, 1418–1421.
10 G. Strinati, *Riv. Nuovo Cimento*, 1988, **11**, 1–86.
11 G. Onida, L. Reining, R. W. Godby, R. Del Sole and W. Andreoni, *Phys. Rev. Lett.*, 1995, **75**, 818–821.
12 L. X. Benedict, E. L. Shirley and R. B. Bohn, *Phys. Rev. B: Condens. Matter Mater. Phys.*, 1998, **57**, R9385–R9387.
13 M. Rohlfing and S. G. Louie, *Phys. Rev. Lett.*, 1998, **80**, 3320–3323.
14 E. L. Shirley, *J. Phys. Chem. Solids*, 2000, **61**, 445–447.
15 E. L. Shirley, *J. Electron Spectrosc. Relat. Phenom.*, 2000, **110-111**, 305–321.
16 E. L. Shirley, J. A. Soininen, G. P. Zhang, J. A. Carlisle, T. A. Callcott, D. L. Ederer, L. J. Terminello and R. C.-C. Perera, *J. Electron Spectrosc. Relat. Phenom.*, 2001, **114-116**, 939–946.
17 J. Vinson, PhD thesis, University of Washington, 2012.
18 J. Vinson, T. Jach, M. Müller, R. Unterumsberger and B. Beckhoff, *Phys. Rev. B*, 2017, **96**, 205116.
19 J. Vinson, T. Jach, M. Müller, R. Unterumsberger and B. Beckhoff, *Phys. Rev. B*, 2019, **100**, 085143.

20 A. Geondzhian and K. Gilmore, *Phys. Rev. B*, 2018, **98**, 214305.
21 E. L. Shirley, *Phys. Rev. Lett.*, 1998, **80**, 794–797.
22 K. Gilmore, J. Vinson, E. L. Shirley, D. Prendergast, C. D. Pemmaraju, J. J. Kas, F. D. Vila and J. J. Rehr, *Comput. Phys. Commun.*, 2015, **197**, 109–117.
23 J. Vinson, T. Jach, M. Müller, R. Unterumsberger and B. Beckhoff, *Phys. Rev. B*, 2016, **94**, 035163.
24 J. A. Carlisle, E. L. Shirley, L. J. Terminello, J. J. Jia, T. A. Callcott, D. L. Ederer, R. C.-C. Perera and F. J. Himpsel, *Phys. Rev. B: Condens. Matter Mater. Phys.*, 1999, **59**, 7433–7445.
25 J. Vinson, J. J. Rehr, J. J. Kas and E. L. Shirley, *Phys. Rev. B: Condens. Matter Mater. Phys.*, 2011, **83**, 115106.
26 P. E. Blöchl, *Phys. Rev. B: Condens. Matter Mater. Phys.*, 1994, **50**, 17953–17979.
27 N. A.-W. Holzwarth, A. R. Tackett and G. E. Matthews, *Comput. Phys. Commun.*, 2001, **135**, 329–347.
28 A. Gulans, S. Kontur, C. Meisenbichler, D. Nabok, P. Pavone, S. Rigamonti, S. Sagmeister, U. Werner and C. Draxl, *J. Phys.: Condens. Matter*, 2014, **26**, 363202.
29 C. Vorwerk, C. Cocchi and C. Draxl, *Phys. Rev. B*, 2017, **95**, 155121.
30 C. Vorwerk, B. Aurich, C. Cocchi and C. Draxl, *Electron. Struct.*, 2019, **1**, 037001.
31 P. A.-M. Dirac and R. H. Fowler, *Proc. R. Soc. London, Ser. A*, 1927, **114**, 710–728.
32 M. van Veenendaal, X. Liu, M. H. Carpenter and S. P. Cramer, *Phys. Rev. B: Condens. Matter Mater. Phys.*, 2011, **83**, 045101.
33 Y. Ma, N. Wassdahl, P. Skytt, J. Guo, J. Nordgren, P. D. Johnson, J.-E. Rubensson, T. Boske, W. Eberhardt and S. D. Kevan, *Phys. Rev. Lett.*, 1992, **69**, 2598–2601.
34 P. D. Johnson and Y. Ma, *Phys. Rev. B: Condens. Matter Mater. Phys.*, 1994, **49**, 5024–5027.
35 J. J. Jia, T. A. Callcott, E. L. Shirley, J. A. Carlisle, L. J. Terminello, A. Asfaw, D. L. Ederer, F. J. Himpsel and R. C.-C. Perera, *Phys. Rev. Lett.*, 1996, **76**, 4054–4057.
36 V. N. Strocov, T. Schmitt, J.-E. Rubensson, P. Blaha, T. Paskova and P. O. Nilsson, *Phys. Status Solidi B*, 2004, **241**, R27–R29.
37 V. N. Strocov, T. Schmitt, J.-E. Rubensson, P. Blaha, T. Paskova and P. O. Nilsson, *Phys. Rev. B: Condens. Matter Mater. Phys.*, 2005, **72**, 085221.
38 Y. Nisikawa, M. Ibuki and M. Usuda, *Phys. B*, 2010, **405**, 1415–1422.
39 L. Hedin, *Phys. Rev.*, 1965, **139**, A796–A823.
40 G. Onida, L. Reining and A. Rubio, *Rev. Mod. Phys.*, 2002, **74**, 601–659.
41 S. Albrecht, G. Onida and L. Reining, *Phys. Rev. B: Condens. Matter Mater. Phys.*, 1997, **55**, 10278–10281.
42 L. X. Benedict, E. L. Shirley and R. B. Bohn, *Phys. Rev. Lett.*, 1998, **80**, 4514–4517.
43 M. Rohlfing and S. G. Louie, *Phys. Rev. Lett.*, 1998, **81**, 2312–2315.
44 J. Vinson and J. J. Rehr, *Phys. Rev. B: Condens. Matter Mater. Phys.*, 2012, **86**, 195135.
45 Y. Noguchi, M. Hiyama, H. Akiyama, Y. Harada and N. Koga, *J. Chem. Theory Comput.*, 2015, **11**, 1668–1673.
46 C. Cocchi, H. Zschiesche, D. Nabok, A. Mogilatenko, M. Albrecht, Z. Galazka, H. Kirmse, C. Draxl and C. T. Koch, *Phys. Rev. B*, 2016, **94**, 075147.
47 F. Fossard, G. Hug, K. Gilmore, J. J. Kas, J. J. Rehr, F. D. Vila and E. L. Shirley, *Phys. Rev. B*, 2017, **95**, 115112.
48 R. Laskowski and P. Blaha, *Phys. Rev. B: Condens. Matter Mater. Phys.*, 2010, **82**, 205104.
49 C. Draxl and C. Cocchi, 2017, arXiv preprint arXiv:1709.02288.
50 W. Olovsson, I. Tanaka, T. Mizoguchi, P. Puschnig and C. Ambrosch-Draxl, *Phys. Rev. B: Condens. Matter Mater. Phys.*, 2009, **79**, 041102.
51 W. Olovsson, I. Tanaka, P. Puschnig and C. Ambrosch-Draxl, *J. Phys.: Condens. Matter*, 2009, **21**, 104205.
52 W. Olovsson, I. Tanaka, T. Mizoguchi, G. Radtke, P. Puschnig and C. Ambrosch-Draxl, *Phys. Rev. B: Condens. Matter Mater. Phys.*, 2011, **83**, 195206.
53 W. Olovsson, L. Weinhardt, O. Fuchs, I. Tanaka, P. Puschnig, E. Umbach, C. Heske and C. Draxl, *J. Phys.: Condens. Matter*, 2013, **25**, 315501.
54 C. Cocchi and C. Draxl, *Phys. Rev. B: Condens. Matter Mater. Phys.*, 2015, **92**, 205105.
55 C. Vorwerk, C. Hartmann, C. Cocchi, G. Sadoughi, S. N. Habisreutinger, R. Félix, R. G. Wilks, H. J. Snaith, M. Bär and C. Draxl, *J. Phys. Chem. Lett.*, 2018, **9**, 1852–1858.
56 K. D. Nanda and A. I. Krylov, *J. Phys. Chem. Lett.*, 2017, **8**, 3256–3265.
57 K. D. Nanda, M. L. Vidal, R. Faber, S. Coriani and A. I. Krylov, *Phys. Chem. Chem. Phys.*, 2020, **22**, 2629–2641.
58 H. R. Phillip and E. A. Taft, *Phys. Rev.*, 1964, **136**, A1445–A1448.
59 R. M. Martin, L. Reining and D. M. Ceperley, *Interacting Electrons: Theory and Computational Approaches*, Cambridge University Press, Cambridge, 2016.
60 F. Bruneval, N. Vast, L. Reining, M. Izquierdo, F. Sirotti and N. Barrett, *Phys. Rev. Lett.*, 2006, **97**, 267601.
61 M. Gatti, F. Sottile and L. Reining, *Phys. Rev. B: Condens. Matter Mater. Phys.*, 2015, **91**, 195137.
62 C. Vorwerk, F. Sottile and C. Draxl, BRIXS, 2021, **https://github.com/exciting/BRIXS**.
63 C. Vorwerk, F. Sottile and C. Draxl, *Phys. Rev. Res.*, 2020, **2**, 042003.
64 C. W. Vorwerk, PhD thesis, Humboldt-Universität zu Berlin, 2021.
65 A. V. Sokolov, E. Z. Kurmaev, S. Leitch, A. Moewes, J. Kortus, L. D. Finkelstein, N. A. Skorikov, C. Xiao and A. Hirose, *J. Phys.: Condens. Matter*, 2003, **15**, 2081–2089.
66 P. H. Hahn, K. Seino, W. G. Schmidt, J. Furthmüller and F. Bechstedt, *Phys. Status Solidi B*, 2005, **242**, 2720–2728.
67 W. Hanke and L. J. Sham, *Phys. Rev. Lett.*, 1974, **33**, 582–585.
68 D. Rocca, Y. Ping, R. Gebauer and G. Galli, *Phys. Rev. B: Condens. Matter Mater. Phys.*, 2012, **85**, 045116.
69 J. A. Soininen and E. L. Shirley, *Phys. Rev. B: Condens. Matter Mater. Phys.*, 2001, **64**, 165112.
70 M. Taillefumier, D. Cabaret, A.-M. Flank and F. Mauri, *Phys. Rev. B: Condens. Matter Mater. Phys.*, 2002, **66**, 195107.

71 F. Pfaff, H. Fujiwara, G. Berner, A. Yamasaki, H. Niwa, H. Kiuchi, A. Gloskovskii, W. Drube, J. Gabel, O. Kirilmaz, A. Sekiyama, J. Miyawaki, Y. Harada, S. Suga, M. Sing and R. Claessen, *Phys. Rev. B*, 2018, **97**, 035110.
72 H. Y. Huang, C. J. Jia, Z. Y. Chen, K. Wohlfeld, B. Moritz, T. P. Devereaux, W. B. Wu, J. Okamoto, W. S. Lee, M. Hashimoto, Y. He, Z. X. Shen, Y. Yoshida, H. Eisaki, C. Y. Mou, C. T. Chen and D. J. Huang, *Sci. Rep.*, 2016, **6**, 1–7.
73 A. L. Fetter and J. D. Walecka, *Quantum Theory of Many-particle Systems*, Dover Publications Inc., 2003.
74 C. D. Clark, P. J. Dean, P. V. Harris and W. C. Price, *Proc. R. Soc. London, Ser. A*, 1964, **277**, 312–329.
75 C. Draxl and M. Scheffler, *MRS Bull.*, 2018, **43**, 676–682.
76 C. Draxl and M. Scheffler, *J. Phys. Mater.*, 2019, **2**, 036001.
77 C. Vorwerk and C. Draxl, *NOMAD Dataset of calculations for diamond*, 2020, **https://dx.doi.org/10.17172/NOMAD/2020**.
78 K. E. Lipinska-Kalita, P. E. Kalita, O. A. Hemmers and T. Hartmann, *Phys. Rev. B: Condens. Matter Mater. Phys.*, 2008, **77**, 094123.
79 J. P. Perdew, A. Ruzsinszky, G. I. Csonka, O. A. Vydrov, G. E. Scuseria, L. A. Constantin, X. Zhou and K. Burke, *Phys. Rev. Lett.*, 2008, **100**, 136406.
80 A. Segura, L. Artús, R. Cuscó, R. Goldhahn and M. Feneberg, *Phys. Rev. Mater.*, 2017, **1**, 024604.
81 J. E. N. Swallow, C. Vorwerk, P. Mazzolini, P. Vogt, O. Bierwagen, A. Karg, M. Eickhoff, J. Schörmann, M. R. Wagner, J. W. Roberts, P. R. Chalker, M. J. Smiles, P. A. E. Murgatroyd, S. A. Razek, Z. W. Lebens-Higgins, L. F. J. Piper, L. A. H. Jones, P. K. Thakur, T.-L. Lee, J. B. Varley, J. Furthmüller, C. Draxl, T. D. Veal and A. Regoutz, 2020, arXiv:2005.13395 [cond-mat].
82 C. Vorwerk and C. Draxl, NOMAD Dataset of calculations for β-Ga_2O_3, 2020, **https://dx.doi.org/10.17172/NOMAD/2020.07.14-4**.

